

# The Impact of Echo Time Shifts and Temporal Signal Fluctuations on BOLD Sensitivity in Presurgical Planning at 7 T

Barbara Dymerska, PhD,\*† Pedro De Lima Cardoso, PhD,\* Beata Bachrata, MSc,\*‡  
 Florian Fischmeister, PhD,\*§|| Eva Matt, MSc,\*§ Roland Beisteiner, MD,\*§  
 Siegfried Trattnig, MD,\* and Simon Daniel Robinson, PhD\*

**Objectives:** Gradients in the static magnetic field caused by tissues with differing magnetic susceptibilities lead to regional variations in the effective echo time, which modifies both image signal and BOLD sensitivity. Local echo time changes are not considered in the most commonly used metric for BOLD sensitivity, temporal signal-to-noise ratio (tSNR), but may be significant, particularly at ultrahigh field close to air cavities (such as the sinuses and ear canals) and near gross brain pathologies and postoperative sites.

**Materials and Methods:** We have studied the effect of local variations in echo time and tSNR on BOLD sensitivity in 3 healthy volunteers and 11 patients with tumors, postoperative cavities, and venous malformations at 7 T. Temporal signal-to-noise ratio was estimated from a 5-minute run of resting state echo planar imaging with a nominal echo time of 22 milliseconds. Maps of local echo time were derived from the phase of a multiecho GE scan. One healthy volunteer performed 10 runs of a breath-hold task. The  $t$ -map from this experiment served as a criterion standard BOLD sensitivity measure. Two runs of a less demanding breath-hold paradigm were used for patients.

**Results:** In all subjects, a strong reduction in the echo time (from 22 milliseconds to around 11 milliseconds) was found close to the ear canals and sinuses. These regions were characterized by high tSNR but low  $t$ -values in breath-hold  $t$ -maps. In some patients, regions of particular interest in presurgical planning were affected by reductions in the echo time to approximately 13–15 milliseconds. These included the primary motor cortex, Broca's area, and auditory cortex. These regions were characterized by high tSNR values (70 and above). Breath-hold results were corrupted by strong motion artifacts in all patients.

**Conclusions:** Criterion standard BOLD sensitivity estimation using hypercapnic experiments is challenging, especially in patient populations. Taking into consideration the tSNR, commonly used for BOLD sensitivity estimation, but ignoring

local reductions in the echo time (eg, from 22 to 11 milliseconds), would erroneously suggest functional sensitivity sufficient to map BOLD signal changes. It is therefore important to consider both local variations in the echo time and temporal variations in signal, using the product metric of these two indices for instance. This should ensure a reliable estimation of BOLD sensitivity and to facilitate the identification of potential false-negative results. This is particularly true at high fields, such as 7 T and in patients with large pathologies and postoperative cavities.

**Key Words:** BOLD sensitivity, clinical fMRI, presurgical planning, local echo time, temporal signal-to-noise ratio, field inhomogeneities

(*Invest Radiol* 2019;54: 340–348)

The use of ultrahigh static magnetic field strength, such as  $B_0 = 7$  T, provides high signal-to-noise ratio (SNR), which in fMRI translates into an enhanced sensitivity to the BOLD effect.<sup>1–4</sup> In addition, the BOLD response also becomes more specific to microvasculature rather than draining veins,<sup>5</sup> improving the localization of activation. Gradient-echo echo planar imaging (EPI), the sequence most commonly used in fMRI, is, however, sensitive to local field inhomogeneities. This increase with  $B_0$  is particularly noticeable close to air/tissue interfaces and is especially prominent in patients with large pathologies or postoperative cavities. Because of these field variations, temporal SNR (tSNR) and effective echo time (TE) are modified. This, in turn, influences BOLD sensitivity, which can be defined as the ability to correctly detect BOLD response from a signal change caused by a local change in  $T_2^*$ .<sup>6</sup>

Hypercapnic experiments such as breath-hold<sup>7</sup> or inhalation of CO<sub>2</sub>-enriched air<sup>8</sup> cause a relatively homogenous increase of cerebral blood flow, which induces a global BOLD signal change in gray matter. Any local variations in  $t$ -maps obtained from such experiments should thus correspond to local BOLD sensitivity change, independent of the origin of this effect. Hypercapnic tasks are, however, very challenging, especially for some patient populations.

The amplitude of BOLD signal change in fMRI is rather small: at 7 T, the change can reach approximately 6% to 8% with primary sensory tasks,<sup>4</sup> but is substantially lower with cognitive<sup>9</sup> and emotional tasks.<sup>10</sup> To detect such small temporal signal fluctuations from a limited number of images with a reasonably high  $t$ -value threshold (ie, to avoid broad-spread false-positive results), high tSNR is required.<sup>11</sup> Temporal SNR is defined as the voxel-wise mean signal over time divided by the signal standard deviation, as an estimate of the noise. Temporal SNR, which incorporates dynamic thermal, technical, and physiological noise sources,<sup>12,13</sup> is a widely used surrogate of BOLD sensitivity.<sup>14–19</sup>

The differing magnetic susceptibilities of tissues close to the base of the brain, auditory canals, and frontal sinuses lead to regional variation in  $B_0$ .<sup>20,21</sup> In patient populations, additional  $B_0$  gradients arise in the proximity of tumors, hemorrhages, metal implants, and postoperative cavities.<sup>22</sup> Strong local gradients in  $B_0$ , that is, those that vary substantially within a voxel, cause signal dephasing and loss. Moderate  $B_0$  gradients, that is, those that are relatively constant within a voxel but

Received for publication October 16, 2018; and accepted for publication, after revision, December 10, 2018.

From the \*High Field Magnetic Resonance Centre, Department of Biomedical Imaging and Image-Guided Therapy, Medical University of Vienna, Vienna, Austria; †Department of Medical Physics and Biomedical Engineering, University College London, London, United Kingdom; ‡CD Laboratory for Clinical Molecular MR Imaging, Vienna; §Study Group Clinical fMRI, Department of Neurology, Medical University of Vienna, Vienna; and ||Institute of Psychology, University of Graz, Graz, Austria.

Conflicts of interest and sources of funding: This study was funded by the Austrian Science Fund (FWF) projects KLI264 and 31452FW. B. Dymerska was additionally supported by a DOC fellowship of the Austrian Academy of Sciences and subsequently by Marie Skłodowska-Curie Action (MRI COMIQSUM #798119). Financial support by the Austrian Federal Ministry for Digital and Economic Affairs and the National Foundation for Research, Technology and Development is likewise gratefully acknowledged.

The authors report no conflicts of interest.

Correspondence to: Simon Daniel Robinson, PhD, High Field Magnetic Resonance Centre, Department of Biomedical Imaging and Image-Guided Therapy, Medical University of Vienna, Lazarettgasse 14/BT32 A-1090, Vienna, Austria. E-mail: simon.robinson@meduniwien.ac.at

Copyright © 2019 The Author(s). Published by Wolters Kluwer Health, Inc. This is an open access article distributed under the Creative Commons Attribution License 4.0 (CCBY), which permits unrestricted use, distribution, and reproduction in any medium, provided the original work is properly cited.

ISSN: 0020-9996/19/5406-0340

DOI: 10.1097/RLI.0000000000000546

vary macroscopically, shift the signal, leading to geometric distortions in image space<sup>21</sup> and changes in the effective TE. For EPI, variations in TE are apparent in  $k$ -space as a shift in the position of the contributions to the echo.<sup>23,24</sup> Signal loss or shortening of the TE cause reduction in BOLD sensitivity, which equates to a reduced ability to detect activation and, potentially, to false-negative results.<sup>25–28</sup> Serious clinical consequences could result from wrong BOLD sensitivity estimation in presurgical mapping if eloquent brain areas were resected because they were not identified as active during the fMRI experiment.<sup>29,30</sup>

Ideally, BOLD sensitivity should be homogeneous throughout gray matter. There are many approaches that try to achieve this by reducing field inhomogeneities using Z-shimming,<sup>31</sup> preparation gradient pulses,<sup>6</sup> or active shimming<sup>32</sup> for instance. There is, however, no shimming technique that can eliminate field inhomogeneities completely. Selection of the most advantageous phase-encoding direction for a given application,<sup>33</sup> voxel size optimization,<sup>34</sup> or slice orientation adjustment to the region of interest<sup>35</sup> have, therefore, been used to reduce the susceptibility-related effects on BOLD sensitivity. Moreover, multiecho acquisitions with weighted combination of images provide high BOLD sensitivity for most parts of the brain.<sup>36</sup> Many other solutions can be found in the literature, but none allows the deleterious effect of field inhomogeneities to be entirely eliminated or corrected. In the light of this enduring problem, the generation of accurate maps of BOLD sensitivity is needed to provide information as to the areas where fMRI can be regarded as reliable, and where not.

Field inhomogeneities modify image signal through increased T2\* dephasing. In addition, modulations in  $B_0$  modify the TE such that it varies throughout the image, depending on the amplitude and sign of susceptibility-induced field gradients. Local changes to the TE increase or decrease the signal depending on whether the TE is reduced or increased, respectively. In EPI, a series of echoes is measured in a long train. The nominal TE is defined as the time from the radiofrequency excitation to the center of  $k$ -space, where, for a perfectly shimmed volume, a collective echo with the highest signal occurs. Such collective echo comprises superimposed echoes from all the spins contributing to the image. Gradients in  $B_0$  cause shifts of the echoes in  $k$ -space causing spreading and splitting of the group of echoes, which correspond to local variations in the TE, that is,  $TE_{local}$ . This effect was first described theoretically by Hutchinson et al<sup>23</sup> for the readout direction and by Haacke et al<sup>24</sup> for the phase encoding direction. The concept was experimentally verified and the field gradients depicted by selection of local groups of echoes in  $k$ -space by Posse et al.<sup>37</sup> Deichmann et al<sup>6</sup> proceeded to depict local TEs on the basis of measured field gradients, defining BOLD sensitivity as the product of the local TE and the magnitude signal:  $BS = TE_{local} \cdot S$ . This definition of BOLD sensitivity has been used in various studies.<sup>35,38,39</sup> Another measure of BOLD sensitivity, the product of tSNR and nominal TE:  $BS = TE_{nominal} \cdot tSNR$ , was introduced by Poser et al<sup>39</sup> and used as a weight in the combination of echoes from multiecho EPI.

To summarize, 4 metrics for BOLD sensitivity estimation, described previously, can be found in the literature. The first is based on hypercapnic experiments, such as breath-hold, and shows BOLD sensitivity variations independent of their origin. It can be thus treated as a criterion standard to which other metrics may be compared. The second assumes that tSNR represents functional sensitivity,<sup>14</sup> neglecting susceptibility-related effects on TE. The third,  $BS = TE_{local} \cdot S$ , incorporates the effect of local variations in the TE but omits temporal variations in the signal.<sup>6</sup> The fourth,  $BS = TE_{nominal} \cdot tSNR$ , accounts for tSNR weighted by the nominal TE (a sequence parameter), but does not incorporate local variations in TE.<sup>39</sup>

In this article, we investigate the size and significance of variations in  $TE_{local}$  and  $tSNR$  in a group of healthy volunteers and patients with brain tumors at 7 T, with a focus on the proximity of pathologies and postoperative cavities, which are frequently encountered in presurgical mapping. Strong susceptibility effects occur in these regions, which could potentially introduce false-negative results.

## MATERIALS AND METHODS

### Image Acquisition

Three healthy volunteers (1 female, average age of  $30 \pm 3$ ) and 11 patients with brain tumors, postoperative cavities, and venous malformations (6 female, average age of  $47 \pm 12$ ) participated in the study, which was approved by the Ethics Committee of the Medical University of Vienna, with written informed consent. Measurements were performed with a 7 T Siemens MAGNETOM scanner (Siemens Healthineers, Erlangen, Germany) and a 32-channel head coil (Nova Medical, Wilmington, MA). Time series SNR was estimated from a 5-minute run of resting state EPI with the following parameters: nominal TE, 22 milliseconds; repetition time TR, 2000 milliseconds; 150 volumes; receiver bandwidth RBW, 1447 Hz/pixel; partial Fourier pF = 6/8; acceleration factor GRAPPA 2; the effective echo spacing (including in-plane acceleration)  $T_{esp}$ , 0.39 milliseconds; matrix size,  $128 \times 128$ , 40 slices; 10% gap; voxel dimensions,  $1.7 \times 1.7 \times 3.0$  mm<sup>3</sup>; flip angle, 70 degrees; and posterior-anterior phase encoding direction. For the calculation of the local TE map, a multiecho GE scan was acquired with the same slice geometry as the EPI and the following parameters: TEs, 5, 10, 16 milliseconds; TR, 658 milliseconds; pF, 6/8; GRAPPA 2; and flip angle, 46 degrees. To establish a criterion standard measure of BOLD sensitivity against which these metrics (ie, local TE and tSNR maps) could be compared, one of the healthy volunteers performed 10 runs of a breath-hold task with the same imaging parameters as in the resting state experiment (other than that 168 volumes were acquired). Each run consisted of 3 breath-hold periods of 30 seconds, preceded by the visual instruction “Inspire,” presented for 2 seconds, and interleaved with 4 off/rest periods of 60 seconds. A less demanding breath-hold paradigm was used for patients, with the following modified timing: 15 seconds breath-hold periods, 3 seconds “Inspire” instruction, 42 seconds rest periods (111 volumes). Ten of eleven patients completed 2 runs of this experiment. Respiration was monitored using a chest belt in both the volunteer and patient studies.

### Data Analysis

Unless otherwise stated, data analysis was performed in MATLAB (version 2013a; MathWorks, Natick, MA). Echo planar imaging runs were coregistered to the third echo of the GE scan (TE = 16 milliseconds), as this had the most similar contrast to the EPI. GE field maps were derived from the phase of the first 2 echoes in the GE scan using the Hermitian inner product.<sup>40</sup> These field maps were subsequently unwrapped with PRELUDE<sup>41</sup> and used to distort-correct the EPI time series using the Voxel Shift Map approach.<sup>42</sup> The mean signal and tSNR were calculated from the unwrapped EPI time series. Field gradients in the phase encoding direction,  $G_y$  in Hz/pixel, were calculated from the field maps and used for the derivation of the local TE maps following the work of Chen et al<sup>43</sup>:

$$TE_{local}(x, y, z) = TE + \Delta TE = TE + \Delta_y(x, y, z) \cdot T_{esp}, \quad [1]$$

with  $\Delta TE$  being the difference between the local and the nominal effective TE and  $\Delta_y(x, y, z)$  defining a shift in the  $k$ -space in the phase-encoding direction:

$$\Delta_y(x, y, z) = \frac{-G_y(x, y, z) \cdot TE}{\frac{1}{M_y} + G_y(x, y, z) \cdot T_{esp}}, \quad [2]$$

where  $T_{esp}$  is the effective echo spacing and  $M_y$  is the matrix size in the phase encoding direction.

The value of  $TE_{local}$  above which the signal falls outside of the  $k$ -space acquisition window, causing so-called type II signal loss,<sup>6</sup> was determined to be 46 milliseconds using,  $TE_{local, max} = T_{esp} \cdot M_y \cdot pF + t_{delay}$ , where  $t_{delay}$  is the total delay between radiofrequency excitation and the beginning of data acquisition ( $t_{delay} = 8.6$  milliseconds for the

GE EPI used). All values for which  $TE_{local}$  is greater than  $TE_{local,max}$  (ie,  $\Delta TE > 24$  milliseconds) were marked (white) on local TE maps to highlight the regions in which complete signal loss was expected and where no conclusion could be drawn about whether there was activation at that position (ie, whether results are true- or false-negative). In addition, the product of scaled  $TE_{local}^{\#} = \frac{TE_{local}}{TE_{nominal}}$  (with the  $TE_{nominal} = 22$  milliseconds) and tSNR was calculated:  $BS = TE_{local}^{\#} \cdot tSNR$ , representing the estimate of BOLD sensitivity, which includes both local variations in TE, as in the work by Deichman et al<sup>6</sup> (ie,  $BS = TE_{local} \cdot S$ ), and temporal variation in signal, as in work by Poser et al<sup>39</sup> (ie,  $BS = TE_{nominal} \cdot tSNR$ ). Scaled values of local TE were used rather than absolute values because it ensures that tSNR and  $TE_{local}^{\#} \cdot tSNR$  will be equal when  $TE_{local} = TE_{nominal}$ .

Regional differences in  $TE_{local}$ , tSNR, and  $TE_{local}^{\#} \cdot tSNR$  maps were assessed using MRIcro (<http://www.cabiatl.com/micro/micro/>).<sup>44</sup> The breath-hold analysis was performed with FSL's FEAT,<sup>45</sup> combining first level (FILM) results for each run in a second-level (FLAME) analysis.

## RESULTS

The correspondence between BOLD sensitivity (for which  $t$ -maps from the breath-hold experiments serve as a surrogate) and the local TE, tSNR, or the product  $TE_{local}^{\#} \cdot tSNR$  is illustrated in Figure 1; results from a healthy volunteer. Regions close to the auditory canals with strongly reduced TE ( $TE_{local} \approx 13$  milliseconds, at arrows in slice 3) have high tSNR (70 and above) and EPI signal, but  $t$ -values close to zero in the breath-hold experiment (Fig. 1, BH  $t$ -map) indicating very low BOLD sensitivity. Here the  $TE_{local}^{\#} \cdot tSNR$  map indices were reduced from 70 to 80 (as in tSNR) to values below 50. To put these results in context, according to Murphy et al,<sup>11</sup> a tSNR of 54 would be required to obtain a significant result with a  $P$  value of 0.001

(typically the most conservative uncorrected  $P$  value used in the literature) and effect size of 1% in a block-designed fMRI experiment with on/off durations similar to those used in the breath-hold experiment in this study. Inclusion of the local TE information, as in the  $TE_{local}^{\#} \cdot tSNR$  metric, shifts the indices below Murphy's value (from 70–80 to below 50). The opposite effect to that described above – regions with long TEs, with good breath-hold response despite low EPI signal and tSNR values – is apparent in slice 5 and, to a lesser extent, over a broad region in slice 7 (at arrows).

Figure 2 shows 4 axial slices of the brain from the same volunteer as in Figure 1 and illustrates strong spatial variations in  $TE_{local}$  and tSNR maps. In slice 3, tSNR was approximately 70 close to the sinuses and ear canals (see the 4 areas marked with arrows), which is relatively high for these regions and above the Murphy value required to obtain significant results (54 under the conditions specified previously). Here, local TE values were reduced to around 11–13 milliseconds, which resulted in  $TE_{local}^{\#} \cdot tSNR$  indices between 35 and 41, that is, below Murphy's value. Close to the ear canals and anterior to the regions with low TE, the  $TE_{local}$  exceeded 46 milliseconds, leading to type II signal loss. These regions are marked in the  $TE_{local}$  and  $TE_{local}^{\#} \cdot tSNR$  maps in white, indicating BOLD sensitivity equal to zero. The map of tSNR showed values around 20 in these areas. Local TE was substantially reduced in the basal ganglia (at white arrows in slice 12) and more dorsally in the parietal lobes (slice 25). In slices 12 and 18, regions with increased local TE (to approximately 31 milliseconds), but with no corresponding local changes in tSNR, are marked with pink arrows. To summarize, even in the healthy brain, field gradients were large enough to lead to substantial changes to the local TE. Reduction in BOLD sensitivity caused by large field gradients was reflected by reduced  $TE_{local}$  and  $TE_{local}^{\#} \cdot tSNR$  values, but not by tSNR, which was increased in these areas due to increase in image signal. There were also regions with increased local TE, which would be expected to have elevated BOLD

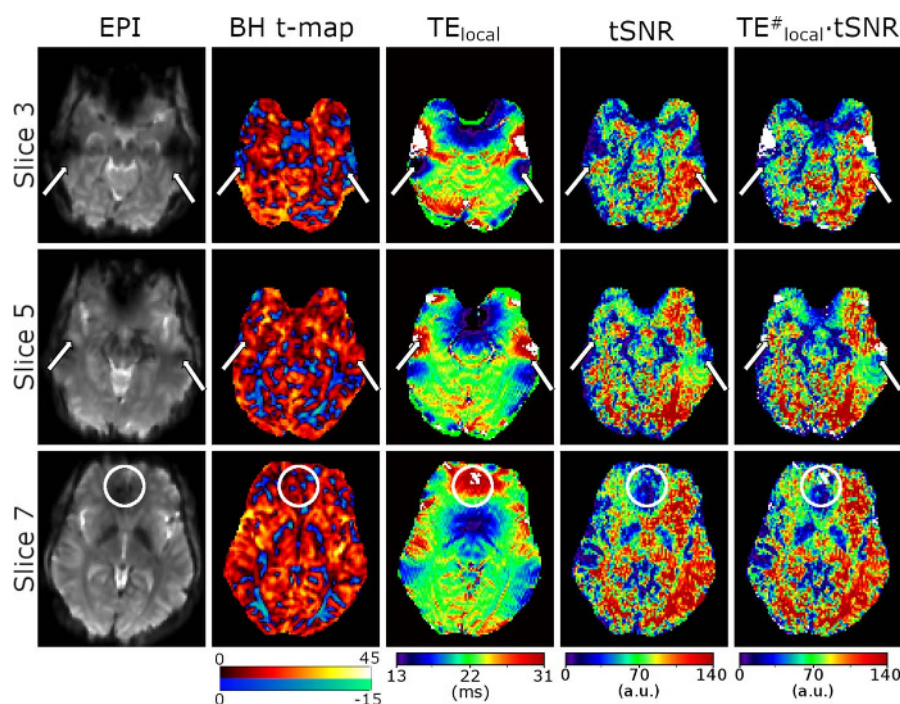


**FIGURE 1.** The results of the hypercapnia experiment with a healthy volunteer showing differences between temporal SNR (tSNR), local echo time, and detected BOLD signal changes in a breath-hold challenge (BH  $t$ -map). Slice 3: The BH  $t$ -map confirms that regions with strongly reduced echo time ( $TE_{local}$ , at arrows) have low BOLD sensitivity despite high tSNR values. Slices 5 and 7 illustrate the contrary effect: the BH  $t$ -map shows that the BOLD sensitivity in regions with strongly positive  $TE_{local}$  (at arrows) is sufficient to detect breathing-related signal changes despite low tSNR. The product metric  $TE_{local}^{\#} \cdot tSNR$  incorporates both local TE and tSNR.

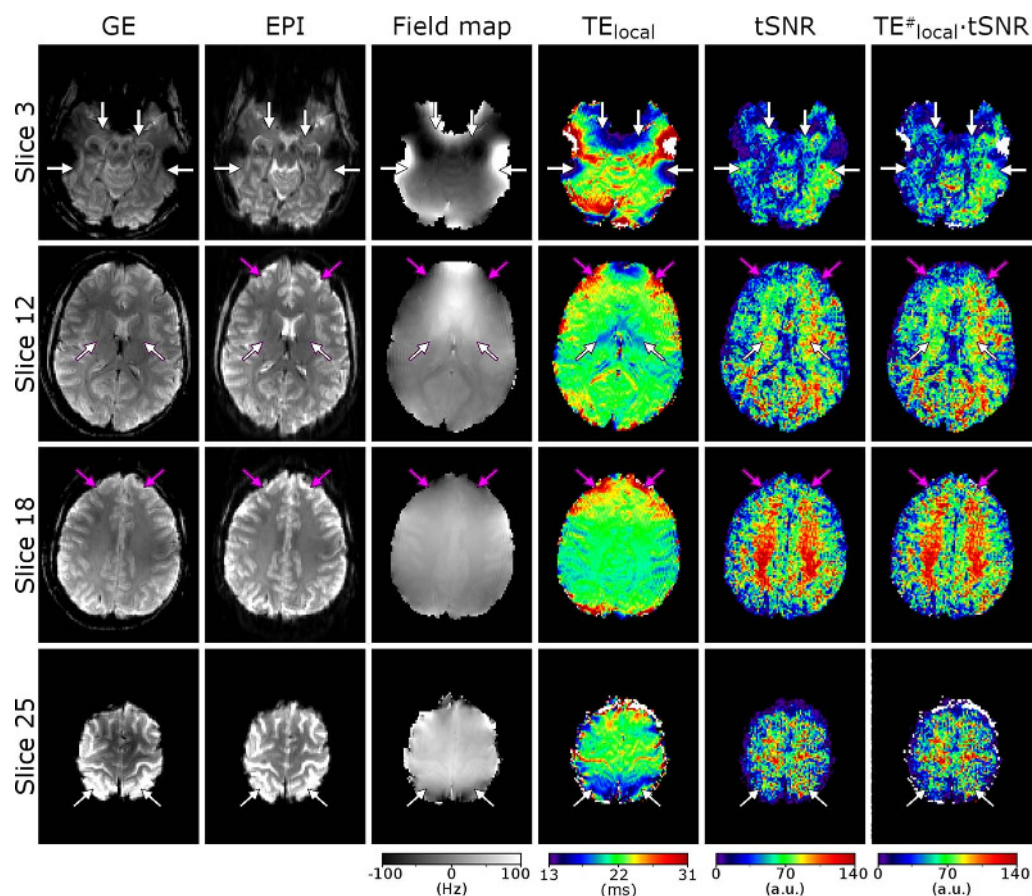


**FIGURE 2.** A comparison of regional variation in echo time ( $TE_{local}$ ), temporal SNR (tSNR), and the product  $TE_{local}^{\#} \cdot tSNR$  maps in a representative healthy volunteer. GE and EPI magnitudes serve as an anatomical reference. A field map shows the field gradients from which local TEs are calculated. Local TE values ranged from 11 milliseconds to in excess of 46 milliseconds, at which time type II signal loss occurred. Strong TE reduction affected, as expected, regions close to ear canals and sinuses (see slice 3, white arrows), but also the basal ganglia and parietal lobes (see white arrows in slice 12 and 25, respectively). Substantial increase in TE was observed not only close to ear canals but also in frontal regions of the brain (see purple arrows in slice 12 and 18).

sensitivity as long as the signal falls within the acquisition window. These were characterized by a decrease in tSNR due to the reduction in image signal.

Discrepancies between local TE and tSNR were more pronounced in the patient group (Fig. 3). For each patient, a slice with strong variation in  $TE_{local}$  close to the pathology and essential brain function was chosen for the visualization of the relevant effects. For Patients 1 and 2, regions in the primary motor cortex were characterized by local TE reduction of up to  $-7$  milliseconds ( $TE_{local} \approx 15$  milliseconds, at arrow positions). In the same regions, tSNR values were relatively high, that is, 70 or above. Combination of the above metrics resulted in  $TE_{local}^{\#} \cdot tSNR$  less than 50. Type II signal losses are flagged in the same figure, for example, in Patient 1, in some frontal and mediolateral areas. In Patient 3, large region near Broca area was characterized by  $TE_{local} \approx 15$  milliseconds. A region near the auditory cortex was similarly affected in Patient 4, where the  $TE_{local} \approx 13$  milliseconds. A strong “dipole-like”  $TE_{local}$  variation can be seen around the postoperative cavity in Patient 5 (at arrow). A region with reduced TE, by up to  $-9$  milliseconds, lies close to the premotor cortex and supplementary motor area, where tSNR values were relatively high (around 80). In Patient 6, regions with reduced TE to 13 milliseconds were observed in the frontal lobes, close to a surgically resected area.

The results for Patients 7 to 11 are presented in Figure 4. In Patient 7, a small region in the primary motor cortex was characterized by  $TE_{local} \approx 19$  milliseconds, tSNR  $\approx 100$ , and  $TE_{local}^{\#} \cdot tSNR \approx 86$ .

The  $TE_{local}$  was substantially increased, to around 31 milliseconds, in Patient 8, in a large region in the frontal lobes, where tSNR was relatively low (around 30). The product metric,  $TE_{local}^{\#} \cdot tSNR$ , increased the indices to 42, which is still below Murphy's value of 54, however. In Patient 9 and 10, small “dipole-like” regions with strongly varying local TE were observed around a postoperative cavity (Patient 9) and around a developmental venous malformation (Patient 10). In Patient 11, a large postoperative cavity caused correspondingly larger changes in  $TE_{local}$  than was the case in Patient 9. In Patients 9, 10, and 11, tSNR was intermediate in value or high (60, 120, and 100, respectively) in regions with reduced TE. To summarize the findings in patients, results were consistent with those in the healthy subject: TE shifts, which modify BOLD sensitivity, were significant and gave complementary information to tSNR maps. Changes in TE were large close to pathologies and postoperative sites. Breath-hold data were acquired for 10 of the 11 patients who participated in the study to provide a criterion standard BOLD sensitivity measure with which tSNR and local TE maps could be compared. These were corrupted by motion artifacts or showed only noisy or not significant signal changes and could not be interpreted.

## DISCUSSION

The purpose of this study was to investigate spatial variations in BOLD sensitivity in healthy volunteers and patients with brain pathologies at 7 T by mapping tSNR and spatial variations in  $TE_{local}$ . In many

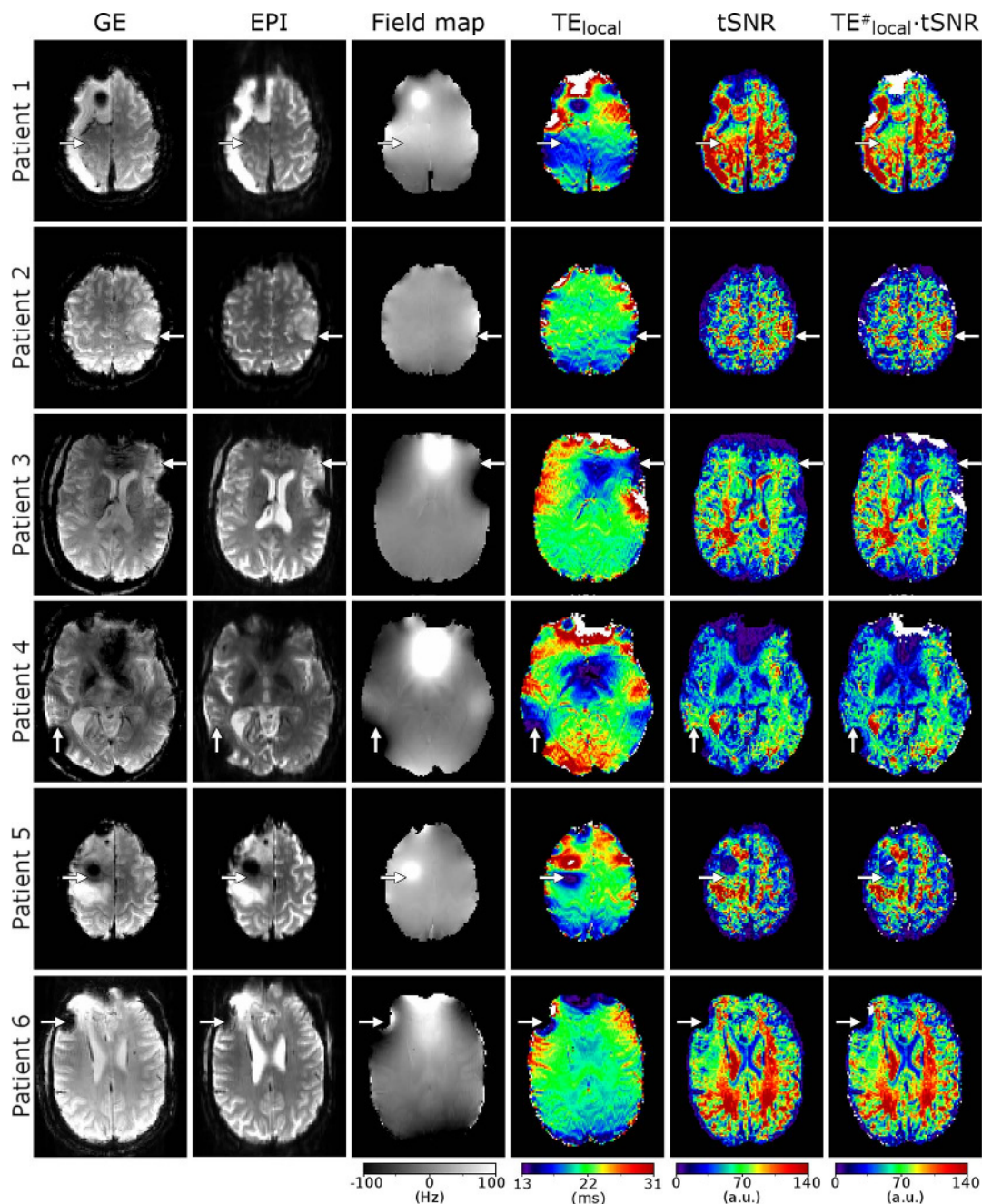


**FIGURE 3.** A comparison of regional variation in echo time ( $TE_{local}$ ), temporal SNR (tSNR), and the product  $TE_{local}^{\#} \cdot tSNR$  maps in Patients 1 to 6. GE and EPI images are shown for anatomical reference. Regions such as primary motor cortex (Patients 1 and 2), Broca area (Patient 3), auditory cortex (Patient 4), premotor cortex and supplementary motor area (Patient 5), and frontal lobes (Patient 6) were characterized by strong reduction in TE but relatively high tSNR (see arrows).

studies, tSNR has been used as an exclusive measure for the detectability of BOLD signal changes.<sup>14–19</sup> Deichmann et al,<sup>6</sup> however, made clear the need to include local variations in TE in the BOLD sensitivity definition:  $BS = TE_{local} \cdot S$ . The current study shows the importance of considering both tSNR and  $TE_{local}$ , by utilizing the product metric of  $TE_{local}^{\#} \cdot tSNR$ , for instance, to obtain a more accurate picture of spatial variations in BOLD sensitivity. Using breath-hold experiments to elicit hypercapnic changes in the BOLD signal, we have shown that where  $TE_{local}$  is low, magnitude images and tSNR may erroneously indicate that there is adequate signal to detect activation, but

BOLD sensitivity is, in fact, too low to do so;  $TE_{local}$  is reduced by susceptibility-induced field gradients, causing the image signal to increase, but functional sensitivity decreases as T2\* contrast has less time to develop. In such regions, tSNR overestimates the BOLD sensitivity as it is proportional to the signal, but is not affected by T2\* contrast changes if calculated from paradigm-free data. Where  $TE_{local}$  is increased, the signal is reduced, but the T2\* contrast increases. Here, tSNR underestimates functional sensitivity unless  $TE_{local}$  is so long that type II signal loss occurs, causing a large drop in tSNR and a fall in signal and BOLD sensitivity to zero. A small residual tSNR value in regions with type

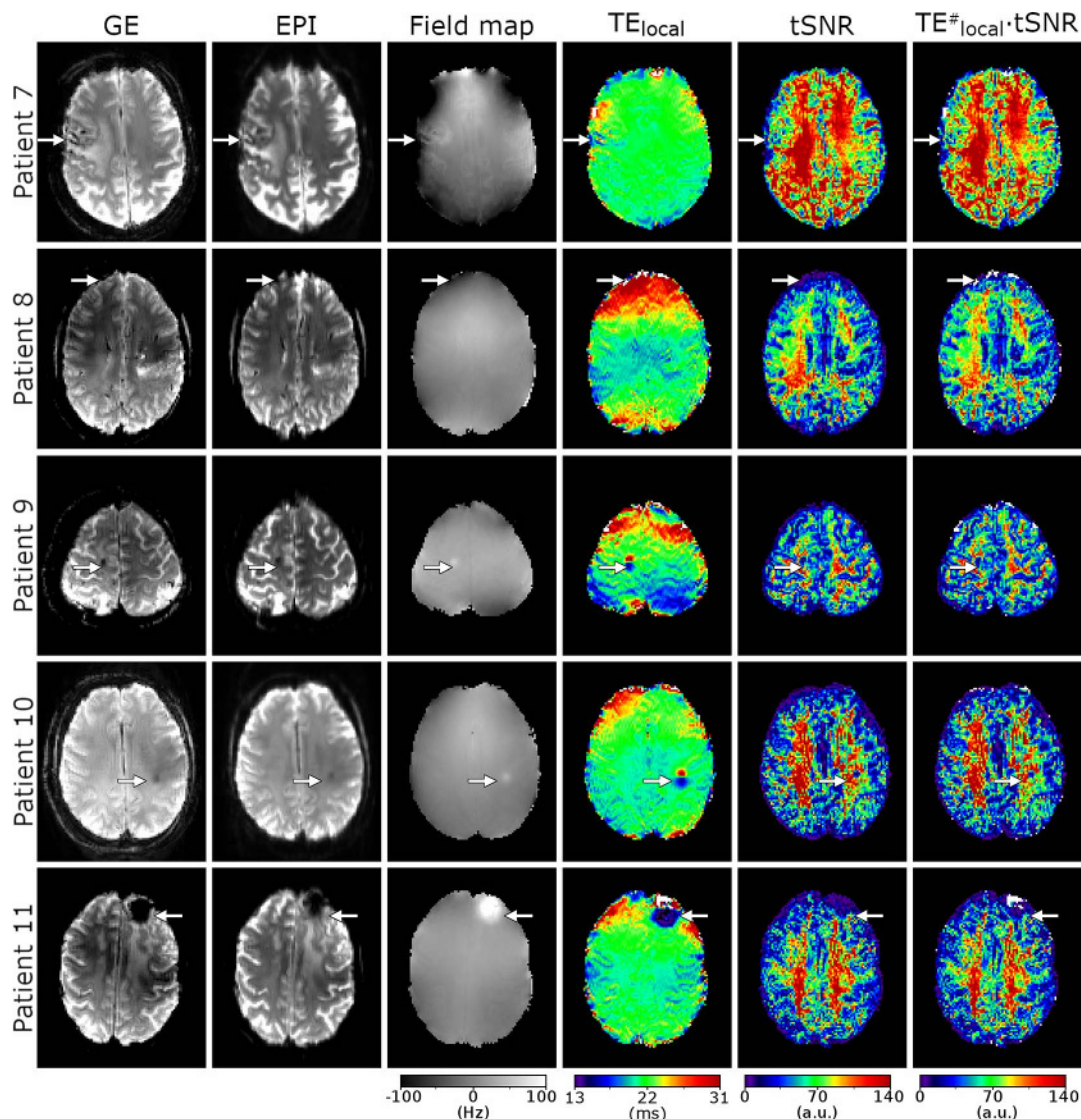


**FIGURE 4.** A comparison of regional variation in echo time ( $TE_{local}$ ), temporal SNR (tSNR), and the product  $TE_{local}^{\#} \cdot tSNR$  maps in Patients 7 to 11. GE and EPI images are shown for anatomical reference. In Patient 7, a small region close to primary motor cortex was characterized by low TE values (see arrow). In Patient 8, a large region in the frontal lobes was affected by increased TE (around 31 milliseconds), but relatively low tSNR (see arrow). In Patients 9 and 11, a dipole-like local TE distribution is apparent around postoperative cavities and in Patient 10 around developmental venous malformation (see arrows). Arrows point to regions with a strong reduction in TE but relatively high tSNR, other than for Patient 8, where an area with increased TE (around 31 milliseconds) and relatively low tSNR is indicated.

II signal loss can occur, because, along with the signal reduction, also noise (which enters in the denominator in tSNR) is reduced – a case described in the Results for Figure 2.

Regions with strongly reduced  $TE_{local}$  (from 22 milliseconds to approximately 11 milliseconds) but relatively high tSNR ( $>70$ ) were found close to the ear canals and sinuses in both healthy volunteers (see Fig. 2) and patients (see Patients 3 and 4 in Fig. 3). The indices of the product metric,  $TE_{local}^{\#} \cdot tSNR$ , were reduced in these regions from 70 (as in tSNR) to 35, which shifts this index from above to below the Murphy value of 54, which is necessary to detect activation for a paradigm similar to the breath-hold experiment used here. Additional regions with substantially reduced local TE (to approximately 13 milliseconds) were found close to pathologies and postoperative cavities in the patient group. This effect was especially prominent in patients with large regions of edema (Patient 2 in Fig. 3), postoperative cavities (Patients 1, 3, 4, 5, and 6 in Fig. 3 and Patient 11 in Figure 4), and close to essential brain

functions such as motor (Patients 1 and 2), language (Patient 3), and auditory areas (Patient 4). This analysis suggests that both  $TE_{local}$  and tSNR should be considered in the analysis of BOLD sensitivity. A product metric of  $TE_{local}^{\#} \cdot tSNR$  may be helpful in this assessment.

The EPI data in this study were acquired with posterior-anterior phase encoding direction. Using the opposite phase encoding polarity (anterior-posterior) causes the gradients in the field to have the opposite sign. In that case, regions in which TE was shortened in this study would be characterized by lengthened TE and vice versa. Both the shortened and the lengthened TE would be expected to correspond to reduced BOLD sensitivity compared with  $TE = T2^*$ , however. Nevertheless, changing phase encoding direction is a simple means by which functional sensitivity can be locally improved if the TE values would otherwise be relatively short in the region of interest.<sup>33</sup> Using alternating phase encoding direction in the course of fMRI experiment might be useful in applications such as resting state network analysis where the

entire gray matter is of interest and certain parts of the brain would benefit from posterior-anterior phase encoding direction, whereas, for others, anterior-posterior phase encoding direction would be advantageous. The use of an alternating phase-encode polarity would, however, require dynamic distortion-correction,<sup>42,46</sup> a careful assessment of other possible effects on signal behavior and the use of high acceleration techniques to significantly reduce the repetition time.

Only field gradients in the phase encoding direction were considered in the calculation of  $TE_{local}$ . Gradients in the readout direction can maximally shift TE by half the echo spacing, which does not significantly shift the echo position.<sup>47</sup>

Echo planar imaging data were acquired with rather thick slices in this study (3 mm) despite the through-plane dephasing which results from this in areas affected by susceptibility effects, particularly at 7 T. Thick slices were used to achieve whole-brain coverage in a reasonable TR, in line with current practice in presurgical planning. There are compelling arguments for using simultaneous multislice (SMS) acceleration<sup>48</sup> to allow an increased number of thinner slices to be acquired with the same repetition time.<sup>49</sup> To our knowledge, however, SMS has, to date, only been adopted in isolated cases in a presurgical planning context, and at lower field.<sup>50</sup> It would be expected that the effects of echo shifts studied here would be yet more apparent when using thin-slice SMS protocols in which intravoxel dephasing is reduced.

Inhalation of CO<sub>2</sub>-enriched air and breath holding has been used to scale task-designed fMRI results, in an effort to account for variations in hemodynamic properties between brain regions.<sup>51,52</sup> Such hypercapnia experiments are affected by both temporal noise sources as well as local TE variations. They are, however, demanding, especially for patient populations, and can introduce a bias due to activation related to the urge to breathe and increased respiratory work.<sup>53</sup> Patient data from breath-hold experiments acquired in this study were very noisy and corrupted by large motion artifacts, supporting the findings of others that this is a highly challenging—if not impractical—undertaking in the clinical setting. Another normalization procedure, based on tSNR maps derived from resting state data, has been used to scale task-designed fMRI results.<sup>54</sup> This does not, however, incorporate susceptibility-induced field effects. In addition, temporal variations in data acquired in the resting state do not only originate from thermal, technical, and physiological noise sources, but also from spontaneous BOLD fluctuations, the frequency and intensity of which can also vary between different brain regions.<sup>55</sup> Utilization of  $TE_{local}$  maps in a normalization procedure in a product with tSNR for instance (ie,  $TE_{local}^{\#} \cdot tSNR$ ) may further reduce the regional variability in the task-related BOLD response, bringing it closer to the actual neuronal activation. Comparison of different normalization procedures is, however, beyond the scope of this article.

Sequences other than gradient-echo EPI have been suggested for fMRI. Spin-echo EPI is less sensitive to susceptibility-related effects than gradient-echo EPI,<sup>56</sup> but is also less sampling-efficient and characterized by higher SAR and reduced functional sensitivity. Spiral-in/out imaging can reduce signal dropout<sup>57</sup> but suffers from image blurring and can require field monitoring and sophisticated reconstruction.<sup>58</sup>

Functional sensitivity estimation can be useful for sequence and acquisition scheme selection: choosing between spin-echo or gradient-echo EPI,<sup>59,60</sup> single-echo or multiecho EPI,<sup>36,39</sup> selecting the number of slices to excite simultaneously in multiband/SMS acquisitions,<sup>48</sup> or in optimizing protocol parameters, such as selecting optimal TE, resolution, flip angle, acceleration factors (with spatially varying g-factors related to them), or phase encoding direction.<sup>35</sup> Correct conclusions can be drawn using the definition of Deichmann et al ( $BS = TE_{local} \cdot S$ ) when comparing measurements in which the signal temporal standard deviation is expected to be equal, as in the study by Weiskopf et al.<sup>35</sup> For protocols with different resolution or acquisition schemes, the tSNR must be included explicitly in the BOLD sensitivity estimation. An additional metric valuable in the comparison of different fMRI acquisition schemes is functional contrast-to-noise ratio, in which the effect size of a specific paradigm

is multiplied by tSNR. This measure is sensitive to both local TE variations, which alter the effect size and temporal signal fluctuations. It is, however, associated with a specific paradigm depending on the intensity of regional stimuli. Functional contrast-to-noise ratio can thus be used as a guideline when selecting the acquisition scheme for a given functional task, but cannot help in evaluating false-negatives and the global, paradigm-independent BOLD sensitivity, unless the effect size is estimated from a hypercapnic experiment.

Local TE values can be used not only to estimate BOLD sensitivity, but also to correct EPI-based  $\Delta B_0$  field maps or T2\* maps. In the expression for  $\Delta B_0$ , the TE occurs in the denominator and is assumed to be univalued throughout the object and equal to the nominal TE.<sup>61</sup> This is generally true for GE-based field maps, where the TE is well defined (with only very small TE variations in the readout direction possible). Strong deviations in TE in EPI may make the correction of EPI-based  $\Delta B_0$  maps by the local TE effects necessary. This could be especially relevant in EPI-based quantitative susceptibility mapping,<sup>62–64</sup> where derived susceptibility values depend on the accuracy of  $\Delta B_0$ . Similarly, in T2\* mapping with EPI, a nominal TE is used for the estimation of the tissue-specific T2\* values,<sup>39,65</sup> although the use of local TE values is more appropriate. The correction of  $\Delta B_0$  and T2\* maps with local TE values pose interesting questions for the future.

Although EPI in this study were distortion-corrected using GE-based field maps, some residual distortions can be seen at the brain boundaries. These occur because static distortion-correction is not accurate in the presence of motion.<sup>66</sup> A dynamic EPI-based field mapping approach could be used,<sup>42,67,68</sup> but local TE effects in  $\Delta B_0$  maps would have to be assessed and corrected to be able to examine the effects of interest in this study, as mentioned in the preceding section. Here, care was taken to compare only regions with a good geometric correspondence between GE and distortion-corrected EPI.

Performing BOLD sensitivity estimation using both  $TE_{local}$  and tSNR maps requires little additional measurement time. In this study, a resting state EPI scan lasting 5 minutes for tSNR estimation and a GE scan with an acquisition time of 30 seconds for the local TE calculation were used. Resting state data is often acquired together with task fMRI to provide complementary information about functional localization,<sup>69</sup> brain connectivity,<sup>70,71</sup> or for the normalization of activation results,<sup>54</sup> and a GE scan is commonly acquired for field mapping-based distortion-correction of functional data.<sup>21,61</sup> We have shown that additional information about potential false-negatives close to pathologies and postoperative cavities can be gained from GE and resting state EPI scans. BOLD sensitivity estimation using  $TE_{local}$  and tSNR is not only attractive for clinical fMRI studies but also in basic neuroscience applications, where in problematic regions, such as the anterior medial-temporal lobe, some of the spatial variability in activation may be explained not by mental processes or physiology<sup>72</sup> but by susceptibility-related effects.

In conclusion, susceptibility-induced field gradients were shown to lead to substantial regional variations in the effective TE at 7 T – from 11 milliseconds to above 46 milliseconds (where type II signal losses occurred) – close to the ear canals and sinuses as well as in the proximity of pathologies and postoperative cavities, near to essential brain functions. Regions with a low effective TE are characterized by a relatively high signal and tSNR. In such cases, considering tSNR but neglecting local changes in TE leads to an overestimation of BOLD sensitivity, as it has been proven using breath-hold experiment as a criterion standard. It is thus important to assess both local changes in the TE and tSNR to obtain reliable BOLD sensitivity estimates and to identify potential false-negative results, particularly in presurgical planning at ultrahigh field.

## REFERENCES

1. Beisteiner R, Robinson S, Wurnig M, et al. Clinical fMRI: evidence for a 7 T benefit over 3 T. *NeuroImage*. 2011;57:1015–1021.

2. Uludağ K, Müller-Bierl B, Uğurbil K. An integrative model for neuronal activity-induced signal changes for gradient and spin echo functional imaging. *Neuroimage*. 2009;48:150–165.
3. Yacoub E, Shmuel A, Pfeuffer J, et al. Imaging brain function in humans at 7 Tesla. *Magn Reson Med*. 2001;45:588–594.
4. van der Zwaag W, Francis S, Head K, et al. fMRI at 1.5, 3 and 7 T: Characterising BOLD signal changes. *Neuroimage*. 2009;47:1425–1434.
5. Duong TQ, Yacoub E, Adriani G, et al. Microvascular BOLD contribution at 4 and 7 T in the human brain: gradient-echo and spin-echo fMRI with suppression of blood effects. *Magn Reson Med*. 2003;49:1019–1027.
6. Deichmann R, Josephs O, Hutton C, et al. Compensation of susceptibility-induced BOLD sensitivity losses in echo-planar fMRI imaging. *Neuroimage*. 2002;15:120–135.
7. Kastrup A, Krüger G, Glover GH, et al. Assessment of cerebral oxidative metabolism with breath holding and fMRI. *Magn Reson Med*. 1999;42:608–611.
8. Rostrup E, Law I, Blinkenberg M, et al. Regional differences in the CBF and BOLD responses to hypercapnia: a combined PET and fMRI study. *Neuroimage*. 2000;11:87–97.
9. Martins MJ, Fischmeister FP, Puig-Waldmüller E, et al. Fractal image perception provides novel insights into hierarchical cognition. *Neuroimage*. 2014;96:300–308.
10. Derntl B, Habel U, Robinson S, et al. Culture but not gender modulates amygdala activation during explicit emotion recognition. *BMC Neurosci*. 2012;13:54.
11. Murphy K, Bodurka J, Bandettini PA. How long to scan? The relationship between fMRI temporal signal to noise ratio and necessary scan duration. *Neuroimage*. 2007;34:565–574.
12. Triantafyllou C, Polimeni JR, Wald LL. Physiological noise and signal-to-noise ratio in fMRI with multi-channel array coils. *Neuroimage*. 2011;55:597–606.
13. Triantafyllou C, Hoge RD, Krueger G, et al. Comparison of physiological noise at 1.5 T, 3 T and 7 T and optimization of fMRI acquisition parameters. *Neuroimage*. 2005;26:243–250.
14. Parrish TB, Gitelman DR, LaBar KS, et al. Impact of signal-to-noise on functional MRI. *Magn Reson Med Off J Soc Magn Reson Med Soc Magn Reson Med*. 2000;44:925–932.
15. LaBar KS, Gitelman DR, Mesulam MM, et al. Impact of signal-to-noise on functional MRI of the human amygdala. *Neuroreport*. 2001;12:3461.
16. Royet J-P, Plailly J, Delon-Martin C, et al. fMRI of emotional responses to odors: influence of hedonic valence and judgment, handedness, and gender. *Neuroimage*. 2003;20:713–728.
17. Small DM, Gregory MD, Mak YE, et al. Dissociation of neural representation of intensity and affective valuation in human gustation. *Neuron*. 2003;39:701–711.
18. Small DM, Gerber JC, Mak YE, et al. Differential neural responses evoked by orthonasal versus retronasal odorant perception in humans. *Neuron*. 2005;47:593–605.
19. Williams LM, Kemp AH, Felmingham K, et al. Trauma modulates amygdala and medial prefrontal responses to consciously attended fear. *Neuroimage*. 2006;29:347–357.
20. Chang H, Fitzpatrick JM. A technique for accurate magnetic resonance imaging in the presence of field inhomogeneities. *IEEE Trans Med Imaging*. 1992;11:319–329.
21. Jezzard P, Balaban RS. Correction for geometric distortion in echo planar images from B0 field variations. *Magn Reson Med*. 1995;34:65–73.
22. Lima Cardoso P, Dymerska B, Bachratá B, et al. The clinical relevance of distortion correction in presurgical fMRI at 7T. *Neuroimage*. 2018;168:490–498.
23. Hutchinson JMS, Sutherland RJ, Mallard JR. NMR imaging: image recovery under magnetic fields with large non-uniformities. *J Phys. [E]*. 1978;11:217.
24. Haacke EM, Tkach JA, Parrish TB. Reduction of T2\* dephasing in gradient field-echo imaging. *Radiology*. 1989;170:457–462.
25. Devlin JT, Russell RP, Davis MH, et al. Susceptibility-induced loss of signal: comparing PET and fMRI on a semantic task. *Neuroimage*. 2000;11:589–600.
26. Veltman DJ, Friston KJ, Sanders G, et al. Regionally specific sensitivity differences in fMRI and PET: where do they come from? *Neuroimage*. 2000;11:575–588.
27. Lipschutz B, Friston KJ, Ashburner J, et al. Assessing study-specific regional variations in fMRI signal. *Neuroimage*. 2001;13:392–398.
28. Robinson SD, Pripfl J, Bauer H, et al. The impact of EPI voxel size on SNR and BOLD sensitivity in the anterior medio-temporal lobe: a comparative group study of deactivation of the Default Mode. *Magn Reson Mater Phys Biol Med*. 2008;21:279–290.
29. Rostomily RC, Berger MS, Ojemann GA, et al. Postoperative deficits and functional recovery following removal of tumors involving the dominant hemisphere supplementary motor area. *J Neurosurg*. 1991;75:62–68.
30. Giovagnoli AR. Quality of life in patients with stable disease after surgery, radiotherapy, and chemotherapy for malignant brain tumour. *J Neurol Neurosurg Psychiatry*. 1999;67:358–363.
31. Glover GH. 3D z-shim method for reduction of susceptibility effects in BOLD fMRI. *Magn Reson Med*. 1999;42:290–299.
32. Wilson JL, Jenkinson M, de Araujo I, et al. Fast, fully automated global and local magnetic field optimization for fMRI of the human brain. *Neuroimage*. 2002;17:967–976.
33. De Panfilis C, Schwarzbauer C. Positive or negative blips? The effect of phase encoding scheme on susceptibility-induced signal losses in EPI. *Neuroimage*. 2005;25:112–121.
34. Robinson S, Windischberger C, Rauscher A, et al. Optimized 3 T EPI of the amygdalae. *Neuroimage*. 2004;22:203–210.
35. Weiskopf N, Hutton C, Josephs O, et al. Optimal EPI parameters for reduction of susceptibility-induced BOLD sensitivity losses: a whole-brain analysis at 3 T and 1.5 T. *Neuroimage*. 2006;33:493–504.
36. Poser BA, Norris DG. Investigating the benefits of multi-echo EPI for fMRI at 7 T. *Neuroimage*. 2009;45:1162–1172.
37. Posse S. Direct imaging of magnetic field gradients by group spin-echo selection. *Magn Reson Med*. 1992;25:12–29.
38. Cusack R, Russell B, Cox SML, et al. An evaluation of the use of passive shimming to improve frontal sensitivity in fMRI. *Neuroimage*. 2005;24:82–91.
39. Poser BA, Versluis MJ, Hoogduin JM, et al. BOLD contrast sensitivity enhancement and artifact reduction with multiecho EPI: parallel-acquired inhomogeneity-desensitized fMRI. *Magn Reson Med*. 2006;55:1227–1235.
40. Bernstein MA, Grbic M, Brosnan TJ, et al. Reconstructions of phase contrast, phased array multicoil data. *Magn Reson Med*. 1994;32:330–334.
41. Jenkinson M. Fast, automated, N-dimensional phase-unwrapping algorithm. *Magn Reson Med*. 2003;49:193–197.
42. Dymerska B, Poser BA, Bogner W, et al. Correcting dynamic distortions in 7T echo planar imaging using a jittered echo time sequence. *Magn Reson Med*. 2016;76:1388–1399.
43. Chen N, Oshio K, Panych LP. Application of k-space energy spectrum analysis to susceptibility field mapping and distortion correction in gradient-echo EPI. *Neuroimage*. 2006;31:609–622.
44. Rorden C. MRICro. Available at: <http://people.cas.sc.edu/rorden/mricro/index.html>. Accessed September 14, 2018.
45. Smith SM, Jenkinson M, Woolrich MW, et al. Advances in functional and structural MR image analysis and implementation as FSL. *Neuroimage*. 2004;23(suppl 1):S208–S219.
46. Andersson JLR, Skare S, Ashburner J. How to correct susceptibility distortions in spin-echo echo-planar images: application to diffusion tensor imaging. *Neuroimage*. 2003;20:870–888.
47. Weiskopf N, Hutton C, Josephs O, et al. Optimized EPI for fMRI studies of the orbitofrontal cortex: compensation of susceptibility-induced gradients in the read-out direction. *Magn Reson Mater Phys*. 2007;20:39–49.
48. Setsompop K, Gagoski BA, Polimeni JR, et al. Blipped-controlled aliasing in parallel imaging for simultaneous multislice echo planar imaging with reduced g-factor penalty. *Magn Reson Med*. 2012;67:1210–1224.
49. Kiss M, Hermann P, Vidnyánszky Z, et al. Reducing task-based fMRI scanning time using simultaneous multislice echo planar imaging. *Neuroradiology*. 2018;60:293–302.
50. Miller KL, Bartsch AJ, Smith SM. Simultaneous multi-slice imaging for resting-state fMRI. *Magnetom Flash*. 2015;70–77.
51. Bandettini PA, Wong EC. A hypercapnia-based normalization method for improved spatial localization of human brain activation with fMRI. *NMR Biomed*. 1997;10:197–203.
52. Handwerker DA, Gazzaley A, Inglis BA, et al. Reducing vascular variability of fMRI data across aging populations using a breathholding task. *Hum Brain Mapp*. 2007;28:846–859.
53. Simon PM, Schwartzstein RM, Weiss JW, et al. Distinguishable sensations of breathlessness induced in normal volunteers. *Am Rev Respir Dis*. 1989;140:1021–1027.
54. Kannurpatti SS, Biswal BB. Detection and scaling of task-induced fMRI-BOLD response using resting state fluctuations. *Neuroimage*. 2008;40:1567–1574.
55. Kalcher K, Boubela RN, Huf W, et al. The spectral diversity of resting-state fluctuations in the human brain. *Plos One*. 2014;9:e93375.
56. Yacoub E, Duong TQ, Van De Moortele PF, et al. Spin-echo fMRI in humans using high spatial resolutions and high magnetic fields. *Magn Reson Med*. 2003;49:655–664.
57. Glover GH, Law CS. Spiral-in/out BOLD fMRI for increased SNR and reduced susceptibility artifacts. *Magn Reson Med*. 2001;46:515–522.

58. Wilm BJ, Barmet C, Gross S, et al. Single-shot spiral imaging enabled by an expanded encoding model: demonstration in diffusion MRI. *Magn Reson Med*. 2017;77:83–91.
59. Naganawa S, Norris DG, Zysset S, et al. Regional differences of fMR signal changes induced by hyperventilation: comparison between SE-EPI and GE-EPI at 3-T. *J Magn Reson Imaging*. 2002;15:23–30.
60. Stroman PW, Krause V, Frankenstein UN, et al. Spin-echo versus gradient-echo fMRI with short echo times. *Magn Reson Imaging*. 2001;19:827–831.
61. Robinson S, Jovicich J. B0 mapping with multi-channel RF coils at high field. *Magn Reson Med*. 2011;66:976–988.
62. Langkammer C, Bredies K, Poser BA, et al. Fast quantitative susceptibility mapping using 3D EPI and total generalized variation. *Neuroimage*. 2015;111:622–630.
63. Sun H, Seres P, Wilman AH. Structural and functional quantitative susceptibility mapping from standard fMRI studies. *NMR Biomed*. 2017;30.
64. Sun H, Wilman AH. Quantitative susceptibility mapping using single-shot echo-planar imaging. *Magn Reson Med*. 2015;73:1932–1938.
65. Speck O, Hennig J. Functional imaging by I0- and T2\*-parameter mapping using multi-image EPI. *Magn Reson Med*. 1998;40:243–248.
66. Jezzard P, Clare S. Sources of distortion in functional MRI data. *Hum Brain Mapp*. 1999;8:80–85.
67. Dymerska B, Poser BA, Barth M, et al. A method for the dynamic correction of B0-related distortions in single-echo EPI at 7T. *Neuroimage*. 2018;168:321–331.
68. Hutton C, Bork A, Josephs O, et al. Image distortion correction in fMRI: a quantitative evaluation. *Neuroimage*. 2002;16:217–240.
69. Langs G, Golland P, Tie Y, et al. Functional geometry alignment and localization of brain areas. *Adv Neural Inf Process Syst Adv Neural Inf Process Syst*. 2010;1:1225–1233.
70. Cole MW, Ito T, Bassett DS, et al. Activity flow over resting-state networks shapes cognitive task activations. *Nat Neurosci*. 2016;19:1718–1726.
71. Schurz M, Wimmer H, Richlan F, et al. Resting-state and task-based functional brain connectivity in developmental dyslexia. *Cereb Cortex N Y NY*. 2015;25:3502–3514.
72. Boubela RN, Kalcher K, Huf W, et al. fMRI measurements of amygdala activation are confounded by stimulus correlated signal fluctuation in nearby veins draining distant brain regions. *Sci Rep*. 2015;5:10499.